X-ray-absorption fine-structure study of ZnSe$_x$Te$_{1-x}$ alloys

J. Pellicer-Porres[a)] and A. Polian
Physique des Milieux Condensés, CNRS-UMR 7602, Université Pierre et Marie Curie, B77
4, place Jussieu, 75252 Paris Cedex 05, France

A. Segura and V. Muñoz-Sanjosé
ICMUV, Univ. de Valencia, c/Dr. Moliner 50, 46100 Burjassot, Valencia, Spain

A. Di Cicco
INFM, Dipartimento di Matematica e Fisica, Università degli studi di Camerino,
Via Madonna delle Carceri, 62032 Camerino (MC), Italy

A. Traverse
Laboratoire pour l'Utilisation du Rayonnement Électromagnétique, Centre Universitaire Paris-Sud,
Bâtiment 209 A, Boîte Postale 34, 91898 Orsay Cedex, France

X-ray-absorption fine-structure experiments at different temperatures in ZnSe$_x$Te$_{1-x}$ (x=0, 0.1, 0.2, 0.55, 0.81, 0.93, 0.99, and 1.0) have been performed in order to obtain information about the structural relaxation and disorder effects occurring in the alloys. First and second neighbor distance distributions have been characterized at the Se and Zn K edges, using multiple-edge and multiple-scattering data analysis. The first neighbor distance distribution was found to be bimodal. The static disorder associated with the Zn–Te distance variance did not depend appreciably on composition. On the other hand, the static disorder associated with the Zn–Se distance increased as the Se content diminished. Using the bonding angle information provided by our experiments the point of view of the anion has been related to that of the cation. The resulting structural model indicates that Zn tetrahedra surrounding the anions remain essentially undistorted, but forced to tilt from their ideal zincblende orientation to accommodate the minority element. The main origin of structural disorder is suggested. © *2004 American Institute of Physics.* [DOI: 10.1063/1.1763989]

I. INTRODUCTION

The development of the first green-blue semiconductor laser[1] was a consequence of the high degree of control of the properties of ZnSe, and advances in doping techniques,[2–4] especially after the introduction of nitrogen as an acceptor using a plasma source.[5,6] These achievements brought a renewed interest in wide gap II-VI semiconductors, as is manifested in the numerous studies about ternary and quaternary alloys (Mg$_y$Zn$_{1-y}$Se$_x$Te$_{1-x}$, ZnS$_x$Te$_{1-x}$, and ZnSe$_x$Te$_{1-x}$, for example), necessary to achieve carrier confinement and optical guide conditions[7–9] utilized in laser diodes based in ZnSe. Due to its applied interest, the band gap dependence on composition has been widely studied.[10–18]

Understanding the band gap (E_g) dependence on composition (x) is also of fundamental interest. The band gap of the AB_xC_{1-x} semiconductor alloys strongly deviates from the average gap of the constituents. This effect, named bowing, is often quantified using a bowing parameter b describing the nonlinear part of $E_g(x)$,

$$E_g(x) = xE_g^{AB} + (1-x)E_g^{AC} - bx(1-x). \qquad (1)$$

The origin of bowing still remains controversial. The so-called band anticrossing model (BAC) has been developed[19] to study bowing in III-V$_x$-N$_{1-x}$ alloys. The model has also been applied to II-VI ternary alloys[12] and,

recently,[13] to the quaternary alloy Mg$_y$Zn$_{1-y}$Se$_x$Te$_{1-x}$. In the BAC model the anion present in less amount in the alloy gives raise to a localized level that interacts with the conduction band minimum, affecting the band gap value.

This model contrasts with more classical approaches[14] where the bowing parameter is decomposed in two terms, $b=b_I+b_{II}$, which represent the nonlinear effects already existing in a fictitious ordered alloy (b_I), and the contribution of disorder itself (b_{II}). b_I may be in turn considered as the sum of three different contributions, $b_I=b_{VD}+b_{CE}+b_S$. The first one, b_{VD}, represents the contribution from volume deformation, and introduces the compression and dilation which is produced in the unit cell of the constituents (AB and AC) to adapt their size to that of the alloy. The second term, b_{CE}, takes into account the possible different chemical electronegativity of the constituents, which may lead to charge redistribution. The third one, b_S, describes structural relaxation that occurs in the alloys. It is well known[20,21] that simple geometrical relationships which exist in pure compounds between bond lengths (R_{AB} and R_{AC}) and lattice constants a_{AB} and a_{AC} ($R=(\sqrt{3}/4)a$ for zincblende, for example) are no longer valid for the alloys. In particular, a bimodal distribution of first neighbor distances is observed.

Information relevant to b_{VD} may be obtained from high pressure x-ray diffraction experiments. We have already begun this type of experiments.[22–24] b_{CE} depends on the inherent properties of B and C. X-ray-absorption fine-structure (XAFS) is sensitive to the local environment of the absorb-

---
[a)]In absence of: ICMUV, Univ. de Valencia, c/Dr. Moliner 50, 46100 Burjassot, Valencia, Spain; electronic mail: Julio.Pellicer@uv.es

ing atoms, and yields information about structural relaxation. in addition, XAFS studies at low temperatures can provide useful information about static disorder. So, XAFS provides essential information about the b_S and b_{II} terms.

A previous XAFS study focused on first neighbor distances.[25] On the other hand, the pair distribution function obtained in Ref. 26 by neutron powder diffraction did not yield information about static disorder, and was not able to discriminate the different next neighbor contributions. We have performed XAFS experiments at different temperatures in the $ZnSe_xTe_{1-x}$ alloy in order to get information about first and next neighbor distances, and associated Debye-Waller factors. We have then constructed a model describing the structural relaxation and disorder effects. The knowledge of these effects is fundamental to assess the problem of gap bowing in the allows.

II. EXPERIMENT

The $ZnSe_xTe_{1-x}$ alloys were grown by physical vapor transport from the binary compounds: ZnSe, was grown by the chemical vapor transport, and ZnTe grown by the cold travelling heater method.[27] The growth method was chosen to ensure random alloying. X-ray diffraction shows the characteristic zincblende pattern. The samples studied correspond to Se concentrations given by $x=1$, 0.99, 0.93, 0.81, 0.55, 0.2, 0.1, and 0. The Se content was inferred from the lattice parameter obtained by x-ray diffraction through Vegard's law (what has been checked for the lattice parameter in Ref. 17).

X-ray-absorption spectra were measured at beamline D42 of the high-energy ring at the Laboratoire pour la Utilisation du Rayonnnement Électromagnétique (LURE). The experiments were performed in the transmission mode, at the Zn (9659 eV) and Se K edge (12 658 eV). We used a Si(111) double-crystal monochromator. The presence of harmonics was avoided using the (111) reflection, and by partial detuning of the monochromator crystals. A reference Cu foil was used to establish the energy calibration. The first inflection point of the Cu foil was set at 8979 eV. The resolution at the Zn and Se K edge was 7.8 and 11.2 eV, respectively.

The alloys were crushed to obtain a fine powder, mixed with cellulose and boron nitride, and pressed in order to form pellets. The mass of sample introduced in each pellet (10 mg/cm^2) was optimized to get the best signal to background ratio at both edges. At the Zn K-edge the total absorption μx ranged from 1.4 to 2, whereas it varied between 1.0 and 1.5 at the Se K-edge.

Samples with a Se content given by $x=0.0$, 0.2, 0.55, 0.81, and 0.99 were mounted in a liquid-helium cryostat, and studied at several temperatures from 10 to 300 K. Alloys with $x=0.1$ and 0.93 were introduced in a liquid-nitrogen cryostat. In this case the spectra were measured at 77 and 300 K.

III. RESULTS AND DISCUSSION

A. XAFS spectra and data analysis

The background subtracted, k-weighted XAFS spectra at the Zn and Se K edge are shown in Fig. 1. Pure ZnSe and ZnTe share the zincblende structure. The Zn cation is sur-
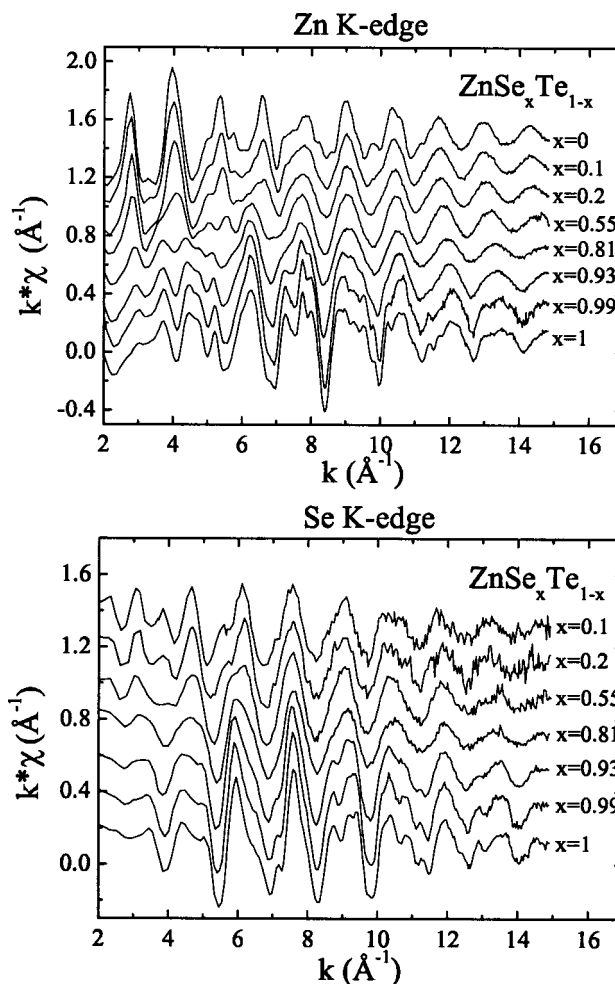

FIG. 1. EXAFS signal of $ZnSe_xTe_{1-x}$ at the Zn and Se K edges. All the spectra have been measured at 77 K, except the ones corresponding to $ZnSe_{0.99}Te_{0.01}$ and $ZnSe_{0.55}Te_{0.45}$, which have been measured at 52 K.

rounded by four Se (ZnSe) or Te (ZnTe) anions situated at $R=(\sqrt{3}/4)a$. In the alloy the Zn environment depends in a direct way on the Se content. The structure of the low k oscillations is specially sensitive to the absorbing atom neighborhood, and it is seen in Fig. 1 that at the Zn K edge their shape vary in a progressive way from ZnSe to ZnTe. On the other hand, the Se first neighbors shell is always formed by four Zn atoms, and the dependence of the Se environment on composition is only from the second shell on, so the low k oscillations are less sensitive to the Se content. The Se environment is directly accessible at all concentrations $x \neq 0$ through the measurements at the Se K edge. However, the jump associated with the Se K edge diminishes with respect to the total absorption as the Se content is reduced, and the spectra become noisier.

The multiple-edge EXAFS analysis was performed using the *ab initio* multiple-scattering (MS) GnXAS package.[28–31] The GnXAS method is based on an n-body expansion of the x-ray absorption crosssection. Within this method, the structural $\chi(k)$ signal is given by a sum of contributions associated with two-body, three-body and higher-order atomic configurations, averaged on the corresponding n-body distributions (g_2, g_3, ...) accounting for thermal and static disorder. The irreducible n-body terms contributing to the

TABLE I. Chalcopyrite ($\bar{I}42d$) model used in the phase shift calculation of Se–Zn*–Te and Se*–Zn–Te three body signals. In our model $a = 5.888$ Å, $c = 2a = 11.776$ Å, $u = (1/4) + [(R^2_{ZnTe} - R^2_{ZnSe})/a^2] = 0.277$.

Atom	Wickoff position	Coordinates
Se	(4a)	(0,0,0)
Te	(4b)	(0,0,1/2)
Zn	(8d)	(u,1/4,1/8)

EXAFS $\chi(k)$ signal are calculated using both MS expansion and continued-fraction techniques,[28,29] and are classified according to the geometry and chemistry of the atomic configurations. In particular, two-body $\gamma^{(2)}$ signals are numbered according to bond distances and type of atoms involved ($\gamma_1^{(2)}$ is associated to the Se first neighbors of Zn, for example). $\gamma^{(3)}$ signals contain the pure three-body contributions associated to triplets of atoms and are also classified according to their geometry. As the definition of a three-body configuration implicitly defines the lower-order two-body ones, it is useful to incorporate the two-body $\gamma_L^{(2)}$ signal associated with the longest distance in the three-body term $\gamma^{(3)}$. This gives the effective MS contribution due to the presence of a second-shell atom, defined as $\eta^{(3)} = \gamma^{(3)} + \gamma_L^{(2)}$.

In this work, the two-body and three-body contributions relevant to ZnSe, ZnTe, and chalcopyrite Zn_2SeTe (see Table I) have been calculated for each atomic edge under consideration. Shown in Table II are the two- and three-body configurations used in the refinements. Each of them has been used only when relevant to either the Zn or Se K edge. The dominant signal is always the first-neighbor two atom signal.

TABLE II. Two- and three-body configurations considered in the XAFS analysis. The three-body configurations are defined by the two shortest bonds, R_{12} and R_{13}, and the angle θ between them. Deg is the number of configurations as a function of the Se composition (x). The starred atoms represent the absorbing atoms. The nomenclature employed to describe the multiple-scattering signals is also given.

Peak	R_{12} (Å)	R_{13} (Å)	θ deg	Deg	Atoms	XAFS sig
			Derived from ZnSe			
g_2						
1	2.458			$4x$	Zn*–Se	$\gamma_1^{(2)}$
				4	Se*–Zn	$\gamma_2^{(2)}$
2	4.014			12	Zn*–Zn	incl. in $\eta^{(3)}$
				$12x$	Se*–Se	incl. in $\eta^{(3)}$
g_3						
1	2.458	2.458	109.5	$12x$	Zn*–Se–Zn	$\eta_1^{(3)}$
				6	Zn–Se*–Zn	$\gamma_2^{(3)}$
2	2.458	2.458	109.5	$6x^2$	Se–Zn*–Se	$\gamma_3^{(3)}$
				$12x$	Se*–Zn–Se	$\eta_4^{(3)}$
			Derived from ZnTe			
$g2$						
3	2.641			$4(1-x)$	Zn*–Te	$\gamma_3^{(2)}$
4	4.313			12	Zn*–Zn	incl. in $\eta^{(3)}$
g_3						
3	2.641	2.641	109.5	$12(1-x)$	Zn*–Te–Zn	$\eta_5^{(3)}$
			Derived from Zn_2SeTe			
g_3						
4	2.461	2.645	109.2	$6x(1-x)$	Se–Zn*–Te	$\gamma_6^{(3)}$
				$12(1-x)$	Se*–Zn–Te	$\eta_7^{(3)}$

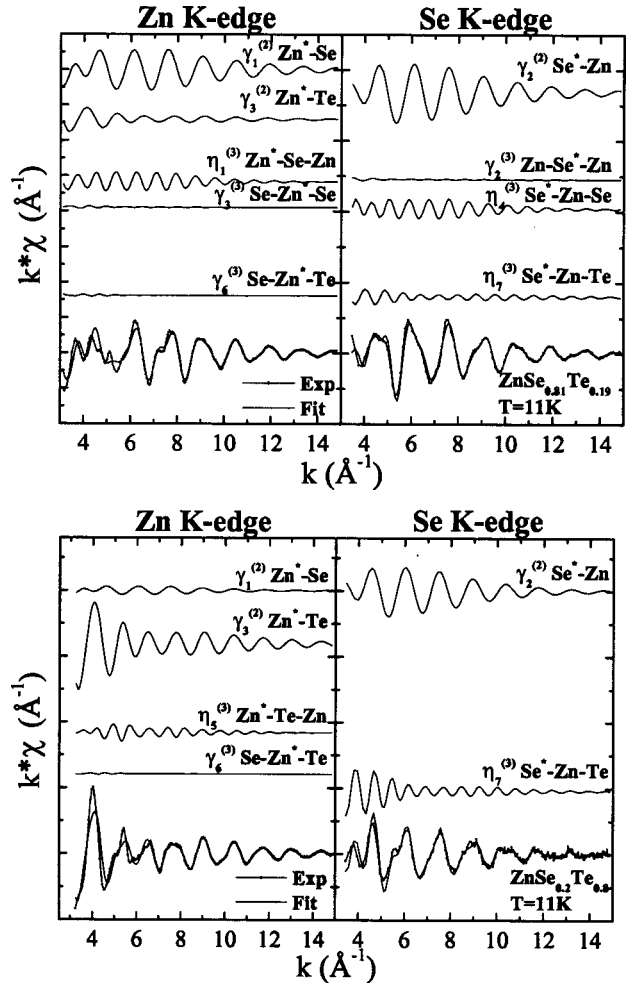FIG. 2. Structural refinement corresponding to $ZnSe_{0.81}Te_{0.19}$ and $ZnSe_{0.2}Te_{0.8}$ spectra at 11 K. The structural fit has been carried out simultaneously at the Zn and Se K edges. In the figure it is shown the decomposition of the multiple scattering into its two-body ($\gamma^{(2)}$), three-body ($\gamma^{(3)}$), and $\eta^{(3)}$ contributions. The $\eta^{(3)}$ signals include the two-body signal corresponding to the longest distance in the triplet.

In the low temperature spectra of slightly alloyed compounds, the second neighbor shells are also relevant.

Data analysis was performed directly on the absorption data without any previous noise filtering or preliminary background substraction. Structural and background parameters were simultaneously obtained minimizing a χ^2-type residual function, following the multiedge method discussed elsewhere.[30–32] The same statistical weight was assigned to the Zn and Se K edges.

The $\gamma^{(2)}$ two-body signals employed in the refinement process to characterize the first shell contribution are defined by their bond distance and associated Debye-Waller factor (see Table II). In the $\gamma^{(3)}$ and η^3 signals, the R_{12} and R_{13} distances describing the shortest bonds in the triplet are identical to first neighbor distances, and do not introduce any new parameter in the fit. θ represents the angle between the shortest bonds in the triplet. R_{12}, R_{13}, and θ completely define the geometry of the triplet, and in particular, in η signals, they establish the R_{23} long distance associated to second neighbors. To complete the characterization of three-body signals, a six parameter symmetric covariance matrix is de-
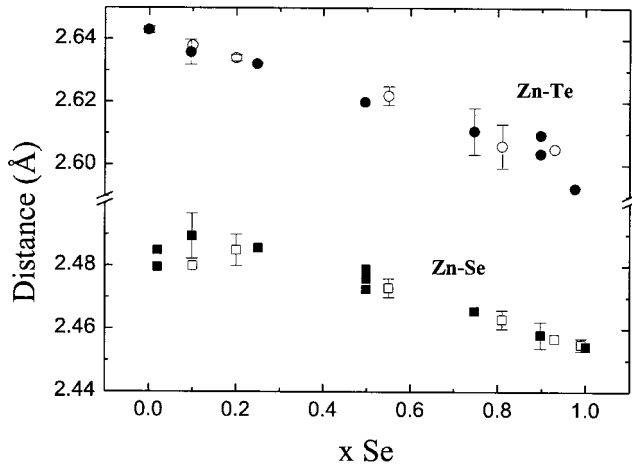
FIG. 3. Hollow symbols: First neighbor Zn−Se and Zn−Te distances in ZnSe$_x$Te$_{1-x}$. Filled symbols: Results from Ref. 25. The original Zn−Te data in Ref. 25 has been shifted 0.006 Å to match the pure ZnTe values.

FIG. 4. Evolution of the Debye-Waller factor as a function of temperature for ZnSe$_{0.99}$Te$_{0.01}$($\square$), ZnSe$_{0.81}$Te$_{0.19}$($\bigcirc$), ZnSe$_{0.55}$Te$_{0.45}$($\triangle$), ZnSe$_{0.2}$Te$_{0.8}$($\diamond$), and ZnTe($\times$). Continuous lines represent fits to Eq. (2).

fined. The covariance matrix contains Debye-Waller factors associated to R_{12} and R_{13} (again identical to that of two-body signals), the angle variance σ_θ, and bond-bond ρ_{RR} and bond-angle $\rho_{R\theta}$ dimensionless correlations. This kind of parametrization is discussed in Ref. 29.

The composition in the first and second shells have been fixed in the analysis, assuming that the alloying is random.

Additional nonstructural parameters considered in the fit are the energy difference between the experimental and theoretical energy scales $\Delta E_0(\text{Zn})$, $\Delta E_0(\text{Se})$; and the amplitude correction factors $S_0^2(\text{Zn})$, $S_0^2(\text{Se})$. The ΔE_0 values are correlated to interatomic distances. They have been determined from the analysis of pure ZnTe and ZnSe spectra, and maintained fixed in all refinements concerning the alloys. The amplitude correction factors are mainly correlated with Debye-Waller factors (σ^2). First of all we performed a preliminary refinement for every composition and temperature with the S_0 considered free. Then the average S_0 value was calculated [$S_0^2(\text{Zn}) = 0.96$ and $S_0^2(\text{Se}) = 1.00$] and introduced in a definitive fit.

Figure 2 gives an example of the structural refinement corresponding to ZnSe$_{0.81}$Te$_{0.19}$ and ZnSe$_{0.2}$Te$_{0.8}$ spectra at 11 K. The theoretical signal has been decomposed into its multiple-scattering components. In the lower part of the figures the agreement between the experimental spectra and the simulations is shown.

B. First neighbors

In Fig. 3 we show (hollow symbols) the first neighbor Zn−Se and Zn−Te distances in the alloys as a function of composition. The Zn−Se distance takes part in the fit at both the Zn and Se K edges. In our fit scheme, where we have fixed the difference ΔE_0 between the experimental and the theoretical energy scales, the main sources of error in the determination of the Zn−Se distance are on the one hand the possible existence of a chemical shift, and on the other the experimental determination of the edge energy. We do not expect the chemical shift to be important as the end compounds are structurally and electronically very similar. In our
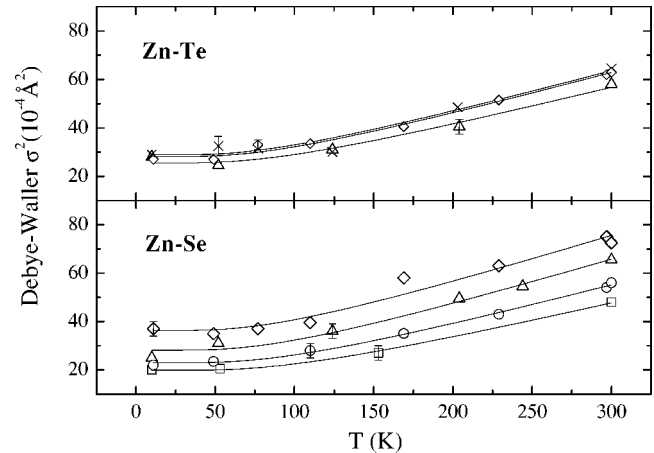
analysis the edge energy is defined by the maximum of the first derivative of the absorption spectrum. The precision of the procedure is ultimately defined by the experimental resolution and the reproducibility of the monochromator position. In contrast, the Zn−Te distance is obtained from a fit to the Zn K edge. As the Te content diminishes the contribution of the $\gamma_3^{(2)}$ Zn−Te signal is reduced with respect to the total one, and the error in the determination of the Zn−Te distance increases. Our measurements are not precise enough to determine the evolution of distances with temperature, which is [33,34] of the order of 0.1% when T varies from 10 to 300 K. However, we can use the distances obtained at different temperatures to estimate statistic errors. In the same figure, XAFS data[25] obtained using pure compounds as structural standards for data analysis is presented as filled symbols. The distances obtained with both analysis are in excellent agreement.

Zn−Se and Zn−Te distances display slow dependence with Se content, and do not follow Vegard's law. The same conclusion has been reached in other alloys since the first observation[20,21] of the phenomenon in Ga$_{1-x}$In$_x$As. XAS studies on liquid pseudobinary ionic alloys[35] have shown that in liquids the first neighbor bimodal distributions do not depend on composition, so the linear dependence observed is considered as a direct lattice effect.

The evolution of Debye-Waler factors as functions of temperature and composition is presented in Fig. 4. It is evident that the dependence of the distance variance on composition is more pronounced in the case of the Zn−Se bond than in the Zn−Te one. In order to analyze both behaviors, the Debye-Waler factors have been decomposed in terms of their static ($\sigma_{A,s}$) and dynamic components ($\sigma_{A,d}$). The dynamic component is described using an Einstein model,

$$\sigma_A^2 = \sigma_{A,s}^2 + \sigma_{A,d}^2 , \tag{2a}$$

$$\sigma_{A,d}^2 = \frac{\hbar}{2\mu_A\omega_A}\coth\left(\frac{\hbar\omega_A}{2kT}\right). \tag{2b}$$

A makes reference to either Zn−Se or Zn−Te. μ_A is the reduced mass, whereas ω_A is a phonon frequency.

J. Appl. Phys., Vol. 96, No. 3, 1 August 2004
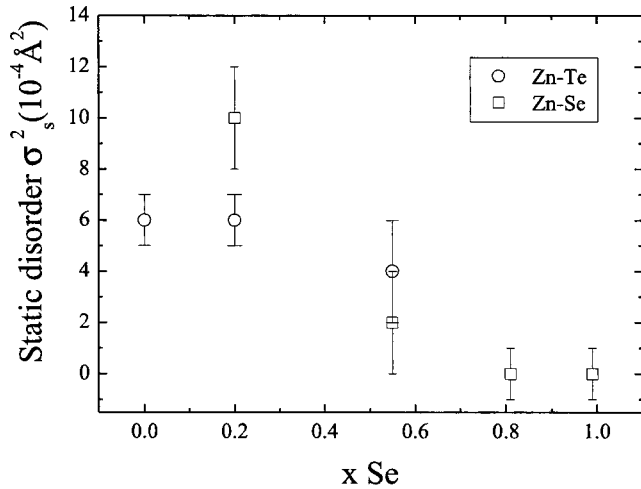
Pellicer-Porres *et al.* 1495

FIG. 5. Evolution of the static disorder contribution to the Debye-Waller factor [see Eq. (2)] associated to first neighbors as a function of the Se content.

The fit of the temperature dependence is presented as continuous lines in Fig. 4. The obtained phonon frequencies increase almost linearly from ZnTe (173 cm^{-1}) to ZnSe (204 cm^{-1}), and are comparable to those of the optic modes[36] in ZnSe ($\omega_{TO}=205$ cm^{-1}, $\omega_{LO}=250$ cm^{-1}) and ZnTe ($\omega_{TO}=177$ cm^{-1}, $\omega_{LO}=205$ cm^{-1}). The static component of the Debye-Waller factor obtained in the fit is reported in Fig. 5. $\sigma_{ZnTe,s}^2$ does not depend appreciably on composition, whereas $\sigma_{ZnSe,s}^2$ clearly increases as the Se content is reduced. It is also important to note that, following Eq. (2), even at low temperature ($2kT \ll \hbar\omega_A$), the static component $\sigma_{A,s}$ represents only a part of the total Debye-Waller.

C. Second neighbors

Second neighbor distances are obtained from the spectra at low temperature, and shown in Fig. 6 as hollow symbols. Zn−Te−Zn and Zn−Se−Zn second neighbor distances obtained in Ref. 25 (filled symbols) are also shown for comparison.

It is apparent the existence of two different behaviors. The Zn−Zn second neighbor distance corresponding to the Zn−Se−Zn and Zn−Te−Zn triplets present a small dependence on concentration, clearly different from that expected from the virtual crystal approximation. The associated bond angle θ (see Table II) remain nearly constant when alloying, although $\theta_{Zn-Te-Zn}$ is found to be smaller than $\theta_{Zn-Se-Zn}$, and closer to the ideal value, 109.47°. On the other hand, the Se−Se and Se−Te second neighbor distances in Se−Zn−Se and Se−Zn−Te present a more pronounced dependence on composition, although not as important as predicted by the virtual crystal approximation (dashed line). In this case we have $\partial\theta_{Se-Zn-Se}/\partial x = -7 \pm 1°$, $\partial\theta_{Se-Ze-Te}/\partial x = -5 \pm 1°$; and θ is reduced as the Se content is increased.

The Debye-Waller factor associated with second neighbors has been calculated using the angle variance σ_θ obtained in the EXAFS fit. Its dependence with temperature has been analyzed using Eq. (2), and the static contribution to the Debye-Waller factor associated with second neighbors has been obtained (see Fig. 7). The cation sublattice appears to
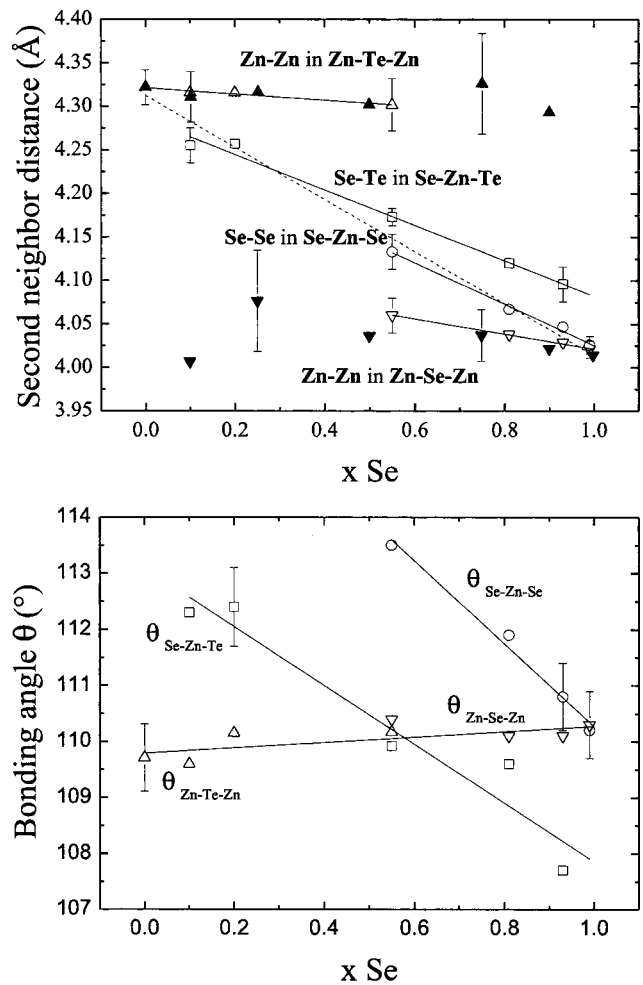

FIG. 6. Upper panel, hollow symbols: second neighbor distance as a function of the Se content x in the ZnSe$_x$Te$_{1-x}$ alloy. Filled symbols: results from Ref. 25. The original Zn−Te−Zn and Zn−Se−Zn data in Ref. 25 have been shifted to match the pure ZnTe and ZnSe values. Lower panel, associated angles (see Table II). Continuous lines represent linear fits. The dashed line corresponds to the virtual crystal approximation.

be the most disordered, and at x=0.55 there is no difference between Zn−Se−Zn and Zn−Te−Zn triplets. As we introduce Te in ZnSe σ_{SeSe}^2 follows σ_{ZnZn}^2, but at x=0.55 it reaches a lower maximum. The behavior of σ_{SeTe}^2 is different, as it is only significative when Se is the minority compound.

D. Structural model

It is widely accepted that the microscopic structure of AB_1C_{1-x} random alloys is different from that of the pure compounds, AB and AC. Perhaps the most striking property is that cation-anion distances show a bimodal distribution, remaining near to that of the end compounds. The ZnSe$_x$Te$_{1-x}$ system is not an exception, as can be appreciated in Fig. 3. To reconcile the existence of two different cation-anion distances with the macroscopic zincblende structure it is necessary to obtain information from farther neighbors. Mikkelsen and Boyce[20,21] found that in Ga$_{1-x}$In$_x$As, the Ga and In second neighbor distance distribution is nearly unimodal, and closely approaches the virtual crystal. On the opposite, the As second neighbor distribution is bimodal, and strongly deviates from the virtual crystal. In the case of
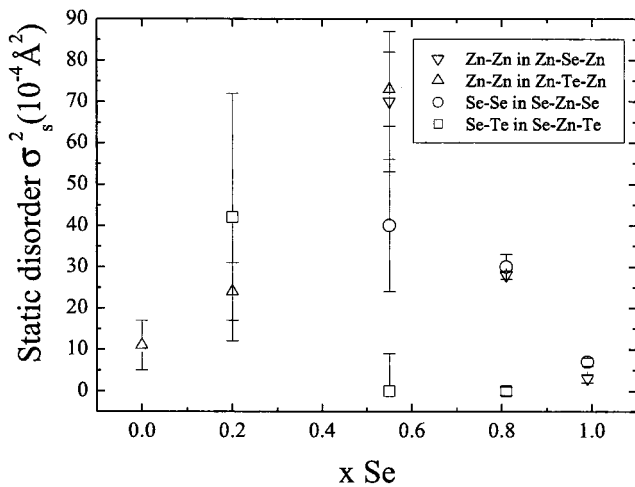
FIG. 7. Evolution of the static disorder contribution to the Debye-Waller factor [see Eq. (2)] associated to second neighbors as a function of the Se content.
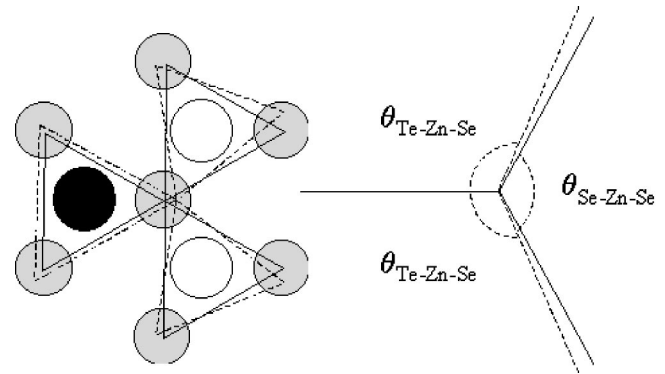

FIG. 8. Structural model describing the substitution of a Se atom (white circles) by a Te one (black circle) in a (111) ZnSe zincblende plane. The Zn atoms are represented by gray circles. The triangles drawn in continuous lines represent the projection of the tetrahedra in the (111) plane before the substitution, whereas the dashed triangles indicate the main distortions after the substitution.

$ZnSe_xTe_{1-x}$ the situation is similar, but with the roles of anions and cations interchanged. In our case the Se–Se and Se–Te distances are close to the virtual crystal, whilst the Zn–Zn distance shows a bimodal distribution (Fig. 6). These differences in behavior indicate[21,37,38] that the Zn sublattice is more likely to be distorted than the anion one. In Fig. 7, the behavior of the static disorder associated with second neighbor distances support this argument, as the static disorder is more important in the cation sublattice than in the anion one. From an intuitive point of view, following Balzarotti *et al.*,[37] if first neighbor interactions are dominant in the alloy it is very likely that Zn atoms, surrounded by different anions, will leave its central position in the tetrahedron. The cation-anion distance has been theoretically investigated using statistical models where all the configurations around the Zn atoms, with 0,1,2,3, or 4 Se atoms, have been taken into account. On the other hand, the anions, which are always surrounded by four identical Zn atoms, should remain in their undistorted positions.

We have tried to relate the information about the cation environment with that of the anion, in order to give a global vision of the alloy. With this in mind we have focused our attention on the angle information provided by our measurements, explicitly introduced in the description of the triplets appearing in Table II. The results suggest that the Zn tetrahedra surrounding the anion remain essentially undistorted, but they are forced to tilt from their ideal zineblende orientations to accommodate the minority compound.

Let us imagine the substitution of a Se atom by a Te one in a Se rich alloy. For simplicity's sake we will concentrate in (111) zincblende planes (Fig. 8). Other planes adequate to represent different Zn displacements are described in Fig. 11 of Ref. 38. Our arguments can be readily extended to those distortions. The tetrahedra where the Se is substituted would be enlarged to accommodate a Zn–Te distance which, according to Fig. 3 is nearly equal (but not exactly) to that of ZnTe. The slight difference is induced by the compressive environment. In a first approximation the substituted Te would be in the center of the tetrahedra, which, as $\theta_{Zn-Te-Zn}$

is maintained constant, would remain essentially undistorted. The presence of the enlarged tetrahedra would force the neighboring tetrahedra to tilt from their ideal positions. In the process $\theta_{Se-Zn-Se}$ would increase and $\theta_{Se-Zn-Te}$ would decrease. Effectively, in Fig. 6, we can see that $\theta_{Se-Zn-Se}$ is bigger, and $\theta_{Se-Zn-Te}$ smaller, than the zincblende value. The same type of reasoning is valid for the substitution of a Te atom by a Se one in a Te rich alloy. Now the Se centered tetrahedra would be contracted, $\theta_{Se-Zn-Te}$ bigger than in zincblende and $\theta_{Te-Zn-Te}$ smaller.

Finally, we can discuss on the origin of static disorder. Let us imagine an anion corresponding to the minority compound in the center of a Zn tetrahedra. A displacement of the anion in the direction of one of the Zn atoms will give origin to the existence of two different cation-anion distances,

$$d_1 = d_0 + h \,, \tag{3a}$$

$$d_2 = \sqrt{h^2 + \frac{h}{\sqrt{6}} d_{Zn-Zn} + \frac{3}{8} d_{Zn-Zn}^2} \cong d_0 - \frac{h}{3} \,, \tag{3b}$$

where $d_0 = (\sqrt{6}/4) d_{Zn-Zn}$ describes the distance from the center to the corners of the tetrahedra, and h is the displacement of the minority compound. If $h > 0$ the anion will approach *three* of the Zn atoms, and will become more separated of the other *one*. We can estimate the static disorder originated as,

$$\sigma_s^2 \cong \frac{h^2}{3}. \tag{4}$$

The precise way in which the minority compounds move inside the tetrahedra depends on energy considerations. As the inner part of the bond potential is harder than the outer one, it should be expected that the anion would approach three of the cations, a $|h|/3$ distance, with the other one becoming a distance $|h|$ further away, rather than in the opposite sense. To estimate the displacement, we have assumed that in a Te rich alloy ($x=0.2$) the Se atom approaches three Zn atoms up to the equilibrium distance in pure ZnSe ($d_2=2.454$ Å). In a Se rich alloy ($x=0.81$) we have supposed that the Te atom moves away from one of the Zn atoms up to the equilibrium distance in ZnTe ($d_1=2.643$ Å). In this way

TABLE III. Estimation of the static disorder generated by small displacements of the minority compound inside the tetrahedra. Energy considerations imply $d_2 < d_0$. In $ZnSe_{0.2}Te_{0.8}$ we have fixed d_2 to that of pure ZnSe. In the same way in $ZnSe_{0.81}Te_{0.19}$ d_1 is estimated from the pureZnTe compound.

x Se	d_0 (Å)	d_1 (Å)	d_2 (Å)	σ_s (Å^2)
		Zn–Se bond		
0.20	2.489	2.595	2.454	0.0037
			(ZnSe)	
		Zn–Te bond		
0.81 (ZnTe)	2.610	2.643	2.600	0.0004

we have calculated the data appearing in Table III, where we see that a greater amount of disorder is generated in the case of the Zn–Se bond than in the Zn–Te one, in agreement with Fig. 5. The ultimate origin of the different shifts of Se and Te atoms is dictated by their different sizes and electronegativities. The substitution of a Te atom by a Se one in a Te rich alloy leaves the Se atom with a certain degree of freedom inside the Zn tetrahedra. The potential well felt by the Se atom is softer than the one felt by a Te atom in a Se rich alloy, where the Te atom is fixed by the compressive environment. These same arguments explain why the second neighbor Debye-Waller factor σ_{SeTe}^2 is small (see Fig. 7) when Te atoms are in low concentration whereas it is of the same order than σ_{SeSe}^2 when the Se content is small.

IV. CONCLUSIONS

In this paper we have described the results of a XAS experiment carried out in $ZnSe_xTe_{1-x}$ (x=0, 0.1, 0.2, 0.55, 0.81, 0.93, 0.99, 1.0) at different temperatures. The structural relaxation and disorder effects occurring in the alloys have been characterized.

First neighbor distances remain near to that of pure compounds, as it is shown in Fig. 3. The second neighbor Zn–Zn distance corresponding to Zn–Se–Zn and Zn–Te–Zn triplets is found to be only slightly dependent on composition. On the other hand, the Se–Se and Se–Te second neighbor distances in Se–Zn–Se and Se–Zn–Te present a more pronounced dependence on composition, although not as important as predicted by the virtual crystal approximation.

Thanks to the angle information provided by our analysis, we have formulated a structural model where the Zn tetrahedra surrounding the anions remain essentially undistorted, but they are forced to tilt from their ideal zincblende orientations to accommodate the minority compound.

The XAS study at different temperatures has allowed us to decompose the Debye-Waller factor into its static and dynamic components. The static disorder associated with the Zn–Te distance variance does not depend appreciably on composition, whereas the static disorder associated with the Zn–Se distance increases as the Se content diminishes. In our model, the substitution of a Te atom by a Se one in a Te rich compound leaves the Se atom with a certain degree of freedom inside the Zn tetrahedra, and results in the main source of static disorder. On the other hand, when a Se atom

is substituted by a Te one in a Se rich compound, the Te atom is maintained at the center of the tetrahedra by the repulsive part of the bonding potential.

We have shown that the use of XAS to study the environment of selected atoms, combined with the utilization of the GnXAS package, constitutes a powerful tool for structural analysis.

[1] M. Haase, J. Qiu, J. DePuydt, and H. Cheng, Appl. Phys. Lett. **59**, 1272 (1991).
[2] M. Haase, H. Cheng, J. DePuydt, and J. Potts, J. Appl. Phys. **67**, 448 (1990).
[3] K. Akimoto, T. Miyajima, and Y. Mori, J. Appl. Phys. **28**, L531 (1989).
[4] T. Yao and Y. Okada, Jpn. J. Appl. Phys., Part 1, **25**, 821 (1988).
[5] R. Park, M. Troffer, C. M. Rouleau, J. DePuydt, and M. Haase, Appl. Phys. Lett. **57**, 2127 (1990).
[6] J. Qiu, J. DePuydt, H. Cheng, and M. Haase, Appl. Phys. Lett. **59**, 2992 (1991).
[7] W. Faschinger, S. Ferreira, and H. Sitter, Appl. Phys. Lett. **64**, 2682 (1994).
[8] T. Baron, K. Saminadayar, and N. Magnea, Appl. Phys. Lett. **67**, 2972 (1995).
[9] P. Mensz, Appl. Phys. Lett. **65**, 2627 (1994).
[10] J. Wu *et al.*, Phys. Rev. B **67**, 035207 (2003).
[11] M.-H. Tsai, S. L. F. C. Peiris, and J. K. Furdyna, Phys. Rev. B **65**, 235202 (2002).
[12] W. Walukiewicz, W. S. K. Yu, J. W. Ager, III, E. Hailer, I. Miotkowski, M. Seong, H. Alawadhi, and A. Ramdas, Phys. Rev. Lett. **85**, 1552 (2000).
[13] J. Wu *et al.*, Appl. Phys. Lett. **80**, 34 (2002).
[14] J. E. Bernard and A. Zunger, Phys. Rev. B **36**, 3199 (1987).
[15] S.-H. Wei and A. Zunger, J. Appl. Phys. **78**, 3846 (1995).
[16] A. Sotto, H. Guder, A. Perez-Pastor, A. Segura, J. Zuñiga, and V. Muñoz, High Press. Res. **22**, 257 (2002).
[17] S. Larach, R. Shrader, and C. Stocker, Phys. Rev. **108**, 587 (1957).
[18] R. Hill and D. Richardson, J. Phys. C **6**, L115 (1973).
[19] W. Shan, W. Walukiewicz, J. W. Ager III, E. Hailer, J. F. Geisz, D. Friedman, J. M. Olson, and S. R. Kurtz, Phys. Rev. Lett. **82**, 1221 (1999).
[20] J. J. C. Mikkelsen and J. B. Boyce, Phys. Rev. Lett. **49**, 1412 (1982).
[21] J. J. C. Mikkelsen and J. B. Boyce, Phys. Rev. B **49**, 7130 (1983).
[22] J. Pellicer-Porres, A. Segura, V. Muñoz, J. Zúñiga, J. P. Itié, A. Polian, and P. Munsch, Phys. Rev. B **65**, 012109 (2001).
[23] J. Pellicer-Porres, A. Segura, J. P. Itié, A. Polian, V. Muñoz, J. Zúñiga, and P. Munsch, High Press. Res. **22**, 355 (2002).
[24] J. Pellicer-Porres, D. Martínez-García, C. Ferrer-Roca, A. Segura, P. Munsch, J. P. Itié, A. Polian, and V. Muñoz-Sanjosé, High Press. Res. **23**, 339 (2003).
[25] J. B. Boyce and J. J. C. Mikkelsen, J. Cryst. Growth **98**, 37 (1989).
[26] P. F. Peterson, T. Proffen, I.-K. Jeong, S. J. L. Billinge, K.-S. Choi, M. G. Kanatzidis, and P. G. Radaelli, Phys. Rev. B **63**, 165211 (2001).
[27] R. Triboulet, K. P. Van, and G. Didier, J. Cryst. Growth **101**, 216 (1990).
[28] A. Filipponi, A. Di Cicco, and C. Natoli, Phys. Rev. B **52**, 15 122 (1995).
[29] A. Filipponi and A. Di Cicco, Phys. Rev. B **52**, 15 135 (1995).
[30] A. Di Cicco, Phys. Rev. B **53**, 6174 (1996).
[31] A. Di Cicco, J. Phys. IV **7**, 171 (1997).
[32] M. Minicucci and A. Di Cicco, Phys. Rev. B **56**, 11 456 (1997).
[33] S. Novikova, Sov. Phys. Solid State **3**, 129 (1961).

[34]S. Novikova and N. Abrisokov, Sov. Phys. Solid State **5**, 1558 (1964).
[35]A. Di Cicco, E. Principi, and A. Filipponi, Phys. Rev. B **65**, 212106 (2002).
[36]M. Cardona, J. Phys. (Paris), Colloq. **8**, 29 (1984).

[37]A. Balzarotti, N. Motta, A. Kisiel, M. Zimnal-Starnawska, M. Czyżyk, and M. Podgórny, Phys. Rev. B **31**, 7526 (1985).
[38]A. Silverman, A. Zunger, R. Kalish, and J. Adler, Phys. Rev. B **51**, 10 795 (1995).